Non-Covalent Matere Bonds in Perrhenates Probed via Ultrahigh Field Rhenium-185/187 NMR and Zero-Field NQR Spectroscopy

COMMUNICATION

Non-Covalent Matere Bonds in Perrhenates Probed via Ultrahigh Field Rhenium-185/187 NMR and Zero-Field NQR Spectroscopy†

Yijue Xu,[a] Miriam Calabrese,[b] Nicola Demitri,[c] Andrea Pizzi,[b] Tamali Nag,[d] Ivan Hung,[a] Zhehong Gan,[a] Giuseppe Resnati[b,*] and David L. Bryce[d,*]

Matere bonds (MaB) to rhenium in a series of organic perrhenates are directly interrogated via $^{185/187}$Re solid-state NMR in applied magnetic fields of up to 35.2 T, and via $^{185/187}$Re NQR spectroscopy. $^{185/187}$Re quadrupolar coupling constants distinguish between MaB samples and control samples, while their precise values are largely governed by the shear strain of the perrhenate anions.

Understanding non-covalent interactions, and the role they play in determining the structure, dynamics, and functional properties of a range of molecules and materials, is of central importance across the chemical and biochemical sciences. In recent years, a unifying concept of element-based electrophilic interactions,[1,2] which builds upon earlier work,[3,4] has gained increased prominence. These interactions are often described within the context of electron donation to σ/π-holes, areas of depleted electron density and elevated electrostatic potential.[5] Most recently, the matere (Ma = Mn, Tc, Re) bond (Fig. 1a) has been identified as a novel structure-directing tool through theoretical analyses and a survey of the Cambridge Structural Database.[6,7,8] This work demonstrated in particular the attractive interaction between group 7 tetroxide anions (MnO$_4^-$, TcO$_4^-$, ReO$_4^-$). The interactions found are consistent with electron donation from a Lewis base into a σ-hole formed opposite one of the Mn/Tc/Re-O covalent bonds, resulting in highly predictable and linear O-Re/Tc/Mn⋯O matere bonds (MaB) which are characterized by reduced distance parameters, N_c, of less than unity. Of particular note in this work is the demonstration that the effect is robust enough to overcome anion-anion repulsion and form MaB between perrhenate anions, forming infinite anion-anion chains.[6]

While X-ray diffraction is invaluable in providing structural information in many cases, other spectroscopic tools must be developed to study non-covalent interactions including MaB. NMR spectroscopy in particular may play an important role in detecting such interactions in cases where diffraction methods may not be apposite.[9] The close link between NMR observables such as chemical shift, *J* coupling, and quadrupolar coupling tensors and the local electronic environment offers an experimental handle for understanding the similarities and differences between various types of non-covalent interactions including the prototypical hydrogen bond. Recent work in this area has focussed on chalcogen bonds,[10] tetrel bonds,[11] pnictogen bonds,[12] and halogen bonds.[13]
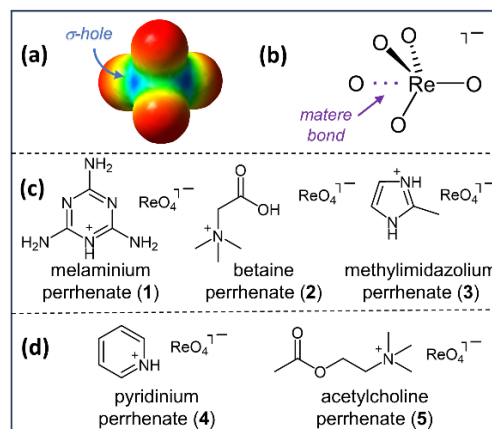
Figure 1. (a) Computed molecular electrostatic potential map for ReO$_4^-$ shows the σ-hole on Re (blue). (b) Matere bond (purple) to a perrhenate anion. Shown below are perrhenates studied herein (c) featuring or (d) not featuring matere bonds.

Here, we report a $^{187/185}$Re (*I* = 5/2) solid-state NMR and nuclear quadrupole resonance (NQR) study of a series of organic perrhenate salts. Three samples (melaminium perrhenate (**1**), betaine perrhenate (**2**), and methylimidazolium

a. *National High Magnetic Field Laboratory, Tallahassee, FL 32310, USA.*
b. *Dept. Chemistry, Materials and Chemical Engineering "Giulio Natta", Politecnico di Milano, Milan, Italy.*
c. *Elettra – Sincrotrone Trieste, 34149 Basovizza, Trieste, Italy.*
d. *Dept. of Chemistry and Biomolecular Sci., University of Ottawa, Ottawa, Canada.*
Correspondence to dbryce@uottawa.ca or giuseppe.resnati@polimi.it

perrhenate (**3**) feature MaB according to their X-ray diffraction structures (Fig. 1b), while pyridinium perrhenate (**4**) and acetylcholine perrhenate (**5**, for which a novel X-ray structure is reported herein[‡]) are control samples which do not feature any MaB (Fig. 1c; Table 1). The acquisition of $^{187/185}$Re solid-state NMR data, and its proper analysis, is notoriously challenging in part due to the large quadrupole moments of both spin-active isotopes and concomitantly enormous spectral broadening even in the highest available applied magnetic fields.[14,15,16]

Table 1. Geometric features of MaB in organic perrhenates

compound	N_c[a]	O-Re···O angle / °	reference
1	0.92	177.74	6
2	0.92	177.09	6
3	0.95	172.66	7
4	n/a[b]	n/a	XUDMIS[17]
5	n/a	n/a	this work

a. N_c is the ratio of the Re···O distance to the sum of the van der Waals radii of Re and O. Radii from Batsanov have been used.[18] b. Not applicable.

Shown in Fig. 2 are $^{185/187}$Re central-transition solid-state NMR spectra of samples **1** to **5**. Shown in Fig. 3 are $^{185/187}$Re NQR

spectra of **2** (see ESI for additional data). The derived quadrupolar coupling and chemical shift tensor parameters are presented in Table 2. The NMR spectra are complicated owing to several factors. Due to the very large $^{185/187}$Re quadrupolar coupling constants, the central transition NMR spectra of perrhenates are known to span several MHz even in very high applied magnetic fields. This means that stepped frequency and/or stepped field approaches must be used to acquire the complete spectra in several parts due to technical limitations on the bandwidth which may be excited and detected in any given experiment. Additionally, the spectra are determined via the complex interplay of chemical shift and quadrupolar coupling tensors, including their generally non-coincident relative orientations.[19] The large quadrupolar interactions mean that standard second-order perturbation theory approaches are inadequate for spectral analysis.[15,20] Finally, the ^{185}Re and ^{187}Re Larmor frequencies are so similar that their spectra overlap. To address these complications, several measures were taken.
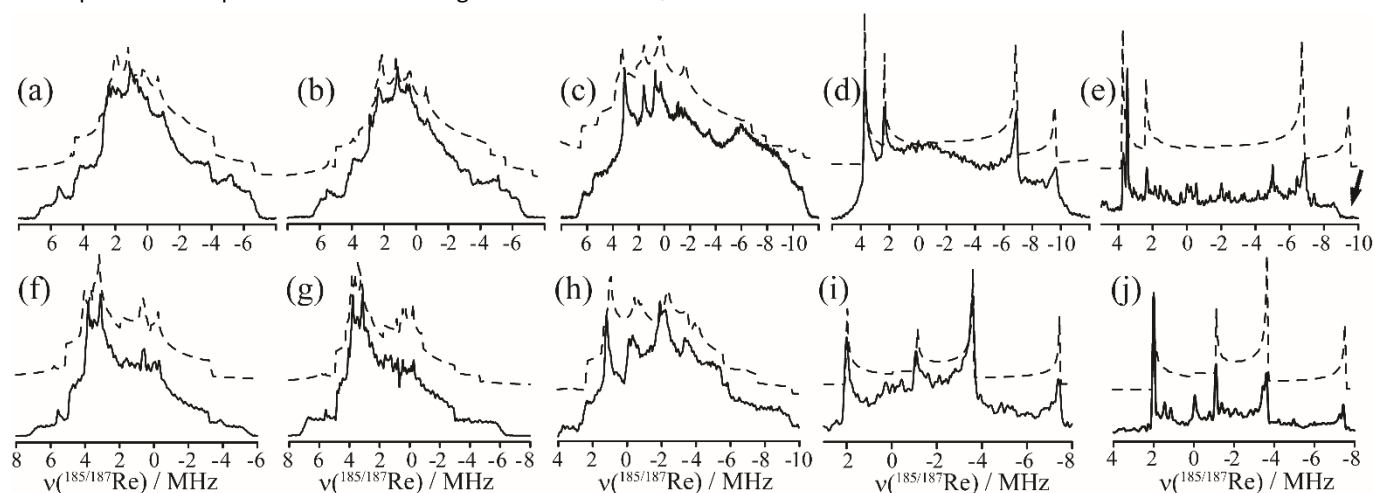
Figure 2. Skyline projections of the experimental (solid black traces) and simulated (dashed black traces) frequency-stepped $^{185/187}$Re QCPMG NMR spectra obtained at 18.8 T (a) **1**, (b) **2**, (c) **3**, (d) **4**, (e) **5**, and field-stepped $^{185/187}$Re QCPMG NMR spectra obtained at 35.2 T (f) **1**, (g) **2**, (h) **3**, (i) **4**, (j) **5**. Data collection in panel (e) was incomplete due to probe arcing at low frequency (see arrow). Data acquired at room temperature. Some inconsistencies due to rf inhomogeneity and probe response across such an enormous spectral range are evident. Note the raised baseline due to the skyline projection.
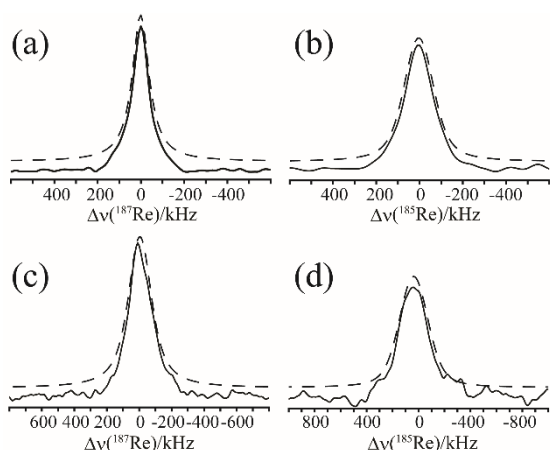
Figure 3. Experimental (solid black traces) and simulated (dashed black traces) ^{187}Re (a, c) and ^{185}Re (b, d) NQR spectra of **2**, acquired with the transmitter on resonance at room temperature. The ^{187}Re transition frequencies are: $\nu_1(m_I = \pm 1/2 \leftrightarrow \pm 3/2) = 44.688$ MHz (a) and $\nu_2(m_I = \pm 3/2 \leftrightarrow \pm 5/2) = 49.334$ MHz (c), where for all transitions $|\Delta m_I| = 1$. The ^{185}Re transition frequencies are: $\nu_1(m_I = \pm 1/2 \leftrightarrow \pm 3/2) = 46.683$ MHz (b) and $\nu_2(m_I = \pm 3/2 \leftrightarrow \pm 5/2) = 51.888$ MHz (d), where for all transitions $|\Delta m_I| = 1$.

Firstly, $^{185/187}$Re NQR spectra were acquired, when possible, to measure quadrupolar frequencies directly, in the absence of the influence of chemical shift anisotropy. This was possible in the case of **1**, **2**, and **3**. For samples **4** and **5**, faster T_2 relaxation apparently rendered the acquisition of NQR spectra impractical. Analysis of the NQR spectra provided two quadrupolar frequencies (ν_1, ν_2) per isotope, which were then analyzed to determine the quadrupolar coupling constant (C_Q) and asymmetry parameter (η). Secondly, NMR data were acquired in two different applied magnetic fields (18.8 T and 35.2 T). The use of such high magnetic fields, in particular the series-connected hybrid (SCH) magnet operating at 35.2 T,[21] offered the most spectral line-narrowing possible. The use of two different applied magnetic fields further increases confidence in the fitting of the spectral data, given the different dependencies of the quadrupolar and chemical shift effects on applied magnetic field strength. Finally, the QCPMG (quadrupolar Carr–Purcell–Meiboom–Gill) sequence of identical excitation and refocusing pulses[22] was used to acquire multiple echoes for

COMMUNICATION

Table 2. Experimental $^{185/187}$Re quadrupolar coupling and chemical shift tensors obtained via exact modelling of the quadrupole interaction[a]

compound	$\|C_Q(^{187}\text{Re})\|$ / MHz	$\|C_Q(^{185}\text{Re})\|$ / MHz	η	δ_{iso}/ ppm	Ω/ ppm	κ	α / °	β / °	γ / °
1	165.86(9)	173.91(5)	0.90(2)	-500(200)	2000(500)	-0.2(3)	120(5)	10(5)	115(10)
2	182.94(2)	192.16(2)	0.88(1)	0(100)	5000(1000)	-0.6(6)	70(2)	46(3)	17(3)
3	225.68(14)	236.88(17)	0.71(2)	1000(200)	6000(500)	-0.6(1)	64(5)	50(3)	15(2)
4	249(1)	263(1)	<0.02	100(200)	<300	--	--	--	--
5	250(1)	264(1)	<0.01	0(100)	<400	--	--	--	--

a. $C_Q = eQV_{33}/h$ where $|V_{33}| \geq |V_{22}| \geq |V_{11}|$ are the principal components of the electric field gradient (EFG) tensor. $\eta = (V_{11}\text{-}V_{22})/V_{33}$; $\delta_{\text{iso}} = (1/3)(\delta_{11} + \delta_{22} + \delta_{33})$; $\Omega = \delta_{11}\text{-}\delta_{33}$; $\kappa = 3(\delta_{22}\text{-}\delta_{\text{iso}})/\Omega$ where $\delta_{11} \geq \delta_{22} \geq \delta_{33}$ are the principal components of the chemical shift tensor. α, β, γ define the relative orientations of the EFG and chemical shift principal axis systems.

sensitivity enhancement. At 18.8 T, variable offset cumulative spectrum data acquisition methods (VOCS)[23] were used to cover the full powder pattern breadth of the final $^{185/187}$Re SSNMR spectra in 73 to 107 steps with an offset increment of 150 to 200 kHz. For the SCH magnet, the conventional frequency-stepped VOCS method is not feasible due to the restricted tuning access for safety reasons. Therefore, the powder pattern was reconstructed by fixing the transmitter frequency and stepping the magnetic field. The subspectra were acquired with B_0 field increment steps varying from 0.013 T to 0.033 T, which correspond to changes in Larmor frequency ranging from 125 to 313 kHz. A final complication is that field stepping is known to not be equivalent to frequency stepping, thus necessitating a more careful spectral analysis.[24] Given the large number of subspectra required to reconstruct the complete $^{185/187}$Re NMR spectra at 35.2 T (up 80 subspectra, see ESI) and the time required to simulate each of these, it was not realistically practical to iteratively simulate these spectra while incorporating the known field-stepping offset as well as the influence of non-coincident NMR interaction tensors. Rather, the exact Zeeman-quadrupolar diagonalization approach implemented in QUEST[20] was used to simulate all spectra. Therefore, some slight shifts in spectral features when comparing the experimental and simulated spectra of Fig.1 are expected for the 35.2 T data.

The ^{187}Re quadrupolar coupling constants measured for the organic perrhenates range from 165.86(9) MHz for **1** to 250(1) MHz for **5** (Table 2). The values of $C_Q(^{185/187}\text{Re})$ for the three samples featuring MaB (**1**, **2**, and **3**) are consistently lower (165.86 to 225.68 MHz) than those for the two control samples which do not feature any MaB (**4** and **5**; 249 and 250 MHz). Similarly, the quadrupolar asymmetry parameter (η) approaches unity for the MaB systems but is essentially zero for the control samples. While the isotropic rhenium chemical shift does not distinguish between the MaB systems and the control samples, likely due to the large errors on these data, the rhenium chemical shift anisotropy does provide another distinguishing parameter. The span (Ω) of the rhenium chemical shift tensor is seen to decrease from thousands of ppm in the cases of **1**, **2** and **3** to almost zero (< 400 ppm) in the control samples. Euler angles (α,β,γ) relating the orientations of the quadrupolar and chemical shift tensor principal axis systems are clearly non-zero in all three compounds featuring matere bonds (Table 2).

Efforts were made to further correlate the rhenium NMR parameters with specific structural features associated with the matere bond. The reduced distance parameter, N_c, does not show significant variation across compounds **1**, **2**, and **3** (Table 1), ranging only between 0.92 and 0.95, and does not correlate with the value of $C_Q(^{187}\text{Re})$. Similarly, the MaB angle remains highly linear and does not correlate with $C_Q(^{187}\text{Re})$. While compounds **1** and **2** feature infinite ReO_4^- anion-anion chains, compound **3** instead features a MaB between ReO_4^- and an oxygen atom of the betaine cation. However, this difference in the identity of the MaB acceptor does not manifest itself in any obvious way in the rhenium NMR data. The explanation for this is that the $^{185/187}$Re NMR parameters are largely governed by the precise coordination geometry of the perrhenate anion itself, namely the lengths of the covalent Re-O bonds and the deviation of the geometry from perfect tetrahedral symmetry. Indeed, gauge-including projector-augmented wave density functional theory (GIPAW DFT) calculations on inorganic perrhenates (for which experimental $C_Q(^{187}\text{Re})$ values range from 134.65(7) MHz for one site in $\text{Ca(ReO}_4)_2\cdot2\text{H}_2\text{O}$ to 251.16(3) MHz in AgReO_4) have shown that deviations in O-Re-O bond angles from perfect tetrahedral symmetry (expressed as shear strain, $|\psi| = \sum|\tan(\theta - 109.47°)|$), rather than Re-O distances, are largely responsible for the range of ^{187}Re quadrupolar coupling constants.[16,‡‡] The present work establishes for the first time a similar trend for matere-bonded organic perrhenates **1**-**3** (Fig. 4).
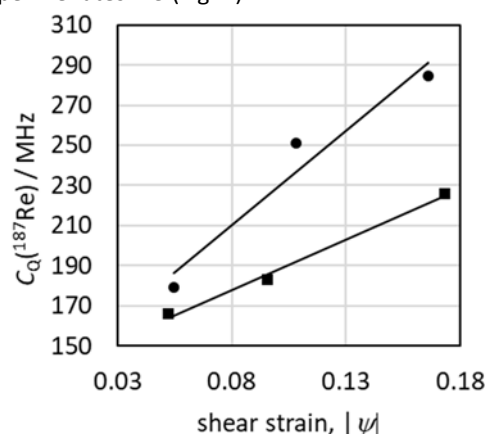
Figure 4. Plot of experimental $C_Q(^{187}\text{Re})$ data against perrhenate anion shear strain for inorganic perrhenates ($\text{Ca(ReO}_4)_2\cdot2\text{H}_2\text{O}$, AgReO_4, KReO_4) (circles; C_Q = 941.49|ψ| + 134.92, R^2 = 0.9469) and organic perrhenates featuring matere bonds (squares; C_Q = 501.07|ψ| + 137.83, R^2 = 0.9931).

It is instructive to compare the present data to those reported for different donor atoms involved in related classes of σ-hole-type non-covalent bonds. For example, $^{35/37}$Cl, $^{79/81}$Br,

COMMUNICATION

Journal Name

and [127]I quadrupolar coupling constants increase upon halogen bond formation to covalently bonded chlorine,[25] bromine,[26] and iodine[27] atoms on substituted halobenzene molecules. However, [121/123]Sb quadrupolar coupling constants instead decrease upon formation of pnictogen bonds to antimony in cocrystals of SbF_3 and $SbCl_3$.[12] In both cases, these trends may be qualitatively understood by considering the loss (in the case of halobenzenes) or increase (in the case of SbX_3) of local symmetry around the donor nucleus. The present case of [185/187]Re quadrupolar coupling constants in perrhenates involved in matere bonds is consistent with the trend seen for pnictogen bonds; however, as emphasized above, the dominant factor for compounds **1**, **2**, and **3**, instead appears to be the shear strain of the ReO_4^- tetrahedron. The primary effect of the matere bond to rhenium on C_Q([185/187]Re) may therefore be indirect, i.e., whereby the MaB contributes to a structural distortion of the ReO_4^- unit, which in turn results in an increase in C_Q. This distortion may be direct and local, or could be the result of the large organic cation influencing the overall crystal packing and symmetry. Further evidence for the role of the MaB in influencing C_Q may be seen by considering that the data for control compounds **4** and **5**, which lack matere bonds, do not follow the same trend with shear strain shown in Fig 4.

As mentioned above, the quadrupolar asymmetry parameter (η) provides a second clearcut distinction between the MaB compounds and the control compounds. The value of $\eta \approx 0$ for compounds **4** and **5**, combined with their particularly short T_2([185/187]Re) values which precluded the acquisition of NQR data, suggests that dynamics may be influencing the NMR spectra. Three-fold hops of the ReO_4^- anion would appear to be consistent with the value of $\eta \approx 0$.[14] Unfortunately, given the technical demands discussed above, it was not feasible to carry out measurements over a range of temperatures to further probe possible dynamic processes. One avenue forward in this regard could involve the study of [17]O-enriched perrhenates[28] via variable-temperature ^{17}O solid-state NMR.

In summary, non-covalent matere bonds have been directly interrogated for the first time via ultrahigh-field [185/187]Re NMR and zero-field NQR spectroscopies, despite many technical challenges. For the organic perrhenates studied herein, values of the rhenium quadrupolar coupling constants, asymmetry parameters, and chemical shift tensor spans differentiate between samples containing MaB and a set of control samples. The impact of the MaB on the NMR spectra is largely indirect, and the trends in quadrupolar coupling constants are more strongly influenced by the shear strain of the ReO_4^- tetrahedra, in line with data for inorganic systems.[16] Given that [185/187]Re have the largest linewidth factors among the stable elements, this work establishes the key roles NMR and NQR can play in probing novel classes of non-covalent interactions even in classically intractable cases of very strong quadrupolar coupling.

Conflicts of interest

There are no conflicts to declare.

Notes and references

‡ Crystallographic data for **5**: (CCDC 2289494): $C_7H_{16}NO_6Re$; $P\overline{1}$; a = 7.313(2) Å, b = 8.956(2) Å, c = 10.153(2) Å; α = 79.13(3)°, β = 71.47(3)°, γ = 67.85(3)°.See ESI for further details.
‡‡ The pronounced sensitivity of GIPAW-DFT Re EFG tensors to a range of effects was shown in reference 16; attempts to compute these data for **1**-**5** did not provide results of any predictive value.
1 G. Cavallo, P. Metrangolo, T. Pilati, G. Resnati and G. Terraneo, *Cryst. Growth Des.*, 2014, **14**, 2697-2702.
2 L. Brammer, A. Peuronen and T. M. Roseveare, *Acta Cryst. C*, 2023, **79**, 204-216.
3 O. Hassel, *Science*, 1970, **170**, 497-502.
4 N. W. Alcock, *Adv. Inorg. Chem. Radiochem.*, 1972, **15**, 1-58.
5 P. Politzer, J. S. Murray, T. Clark and G. Resnati, *Phys. Chem. Chem. Phys.*, 2017, **19**, 32166-32178.
6 A. Daolio, A. Pizzi, G. Terraneo, A. Frontera and G. Resnati, *ChemPhysChem*, 2021, **22**, 2281-2285.
7 A. Daolio, A. Pizzi, M. Calabrese, N. Demitri, J. S. Murray, P. Politzer and G. Resnati, *Cryst. Growth Des.*, 2023, **23**, 574-579.
8 S. Burguera, R. M. Gomila, A. Bauzá and A. Frontera, *Crystals*, 2023, **13**, 187.
9 Y. Xu, P. M. J. Szell, V. Kumar and D. L. Bryce, *Coord. Chem. Rev.*, 2020, **411**, 213237.
10 V. Kumar, Y. Xu, C. Leroy and D. L. Bryce, *Phys. Chem. Chem. Phys.*, 2020, **22**, 3817-3824.
11 S. A. Southern, T. Nag, V. Kumar, M. Triglav, K. Levin and D. L. Bryce, *J. Phys. Chem. C*, 2022, **126**, 851-865.
12 C. Leroy, R. Johannson and D. L. Bryce, *J. Phys. Chem. A*, 2019, **123**, 1030-1043.
13 J. Viger-Gravel, S. Leclerc, I. Korobkov and D. L. Bryce, *J. Am. Chem. Soc.*, 2014, **136**, 6929-6942.
14 R. W. Schurko, S. Wi and L. Frydman, *J. Phys. Chem. A*, 2002, **106**, 51-62.
15 C. M. Widdifield, A. D. Bain and D. L. Bryce, *Phys. Chem. Chem. Phys.*, 2011, **13**, 12413-12420.
16 C. M. Widdifield, F. A. Perras and D. L. Bryce, *Phys. Chem. Chem. Phys.*, 2015, **17**, 10118-10134.
17 P. Czarnecki and H. Maluszynska, *J. Phys.:Condens. Matter*, 2000, **12**, 4881-4892.
18 S. S. Batsanov, *Inorg. Materials*, 2001, **37**, 871-885.
19 D. L. Bryce, Tensor Interplay, in 'Encyclopedia of Magnetic Resonance'; R. K. Harris and R. E. Wasylishen, Eds.; Wiley (2008).
20 F. A. Perras, C. M. Widdifield and D. L. Bryce, *Solid State Nucl. Magn. Reson.*, 2012, **45-46**, 36-44.
21 Z. Gan, I. Hung, X. Wang, J. Paulino, G. Wu, I. M. Litvak, P. L. Gor'kov, W. W. Brey, P. Lendi, J. L. Schiano, M. D. Bird, I. R. Dixon, J. Toth, G. S. Boebinger and T. A. Cross, *J. Magn. Reson.*, 2017, **284**, 125-136.
22 F. H. Larsen, J. Skibsted, H. J. Jakobsen and N. C. Nielsen, *J. Am. Chem. Soc.*, 2000, **122**, 7080-7086.
23 D. Massiot, I. Farnan, N. Gautier, D. Trumeau, A. Trokiner and J. P. Coutures, *Solid State Nucl. Magn. Reson.*, 1995, **4**, 241-248.
24 I. Hung, A. Altenhof, R. W. Schurko, D. L. Bryce, O. Han and Z. Gan, *Magn. Reson. Chem.*, 2021, **59**, 951-960.
25 P. M. J. Szell and D. L. Bryce, *J. Phys. Chem. C*, 2016, **120**, 11121-11130.
26 P. Cerreia Vioglio, P. M. J. Szell, M. R. Chierotti, R. Gobetto and D. L. Bryce, *Chem. Sci.*, 2018, **9**, 4555-4561.
27 P. M. J. Szell, L. Grébert and D. L. Bryce, *Angew. Chem. Intl. Ed.*, 2019, **58**, 13479-13485.
28 H. J. Jakobsen, H. Bildsøe, M. Brorson, Z. Gan and I. Hung, *J. Magn. Reson.*, 2013, **230**, 98-110.